DATASETS OF STRATIFICATION OF CATHODE CATALYST LAYERS IN LOW-TEMPERATURE PROTON EXCHANGE MEMBRANE FUEL CELLS

Zikhona Nondudule [1], Jessica Chamier [2,*] and Mahabubur Chowdhury [1]

[1] Department of Chemical Engineering, Faculty of Engineering, Cape Peninsula University of Technology, Cape Town 7530, South Africa; 210237058@cput.ac.za
[2] Department of Chemical Engineering, Centre for Catalysis Research, HySA Catalysis, University of Cape Town, Cape Town 7700, South Africa; jessica.chamier@uct.ac.za
* jessica.chamier@uct.ac.za; Tel.: +27 (0) 21 6502515

Abstract: To decrease the cost of fuel cell manufacturing, the amount of Pt in the catalyst layer needs to be reduced. In this study, ionomer gradient membrane electrode assemblies (MEAs) were designed to reduce Pt loading without sacrificing performance and lifetime. A two-layer stratification of the cathode was achieved with varying ratios of 28 wt% ionomer in the inner layer, on the membrane, and 24wt% on the outer layer, coated onto the inner layer. To study the MEA performance, the electrochemical surface area (ECSA), polarization curves, and electrochemical impedance spectroscopy (EIS) responses were evaluated under 20 %, 60 %, and 100 % relative humidity (RH). The stratified MEA Pt loading was reduced by 12 % while maintaining commercial equivalent performance. The optimal two-layer design was achieved when Pt loading ratio between the layers was 1:6 (inner: outer layer). This MEA showed the highest ECSA and performance at 0.65 V with reduced mass transport losses. The integrity of stratified MEAs with lower Pt loading was evaluated with potential cycling and proved more durable than the monolayer MEA equivalent. The higher ionomer loading adjacent to the membrane and the bi-layer interface of the stratified catalyst layer (CL) increased moisture in the cathode CL, decreasing the degradation rate. Using ionomer stratification to decrease the Pt loading in a MEA yielded better performance compared to the monolayer MEA design. This study therefore contributes to the development of more durable, cost-effective MEAs for low-temperature proton exchange membrane fuel cells.

Keywords: Proton exchange membrane fuel cell; Cathode catalyst layers; Ionomer loading; Stratified cathode catalyst layers.

1. Introduction

Proton exchange membrane fuel cells (PEMFCs) have attracted great attention in research and development because of its simplicity, low temperature operation (50-100 °C) and higher power density (40%-60%) with the absence of pollutants [1]. PEFCs currently use platinum (nanoparticles dispersed on carbon support) as catalysts for the energy driving hydrogen oxidation reaction (HOR) and oxygen reduction reaction (ORR) which significantly increases their manufacturing cost [2]. The ORR occurring at the cathode is about 6 orders of magnitude slower than the HOR requiring a higher Pt loading and is therefore the focal point for Pt reduction. Research and development activities are therefore aimed at improving the catalyst activity and utilization in the cathode catalysts layer (CCL) without compromise in the durability and stability [3].

A promising membrane electrode assembly (MEA) design includes the development of graduated multilayer catalyst layers in the catalyst coated membrane (CCM). Graduated CCL structure can increase the Pt catalyst use efficiency by increasing the available Pt surface area. Recent studies have shown O_2 mass transport resistance to be inversely proportional to Pt loading and highly dependent on the available Pt surface area [4].

Many studies have focused on the CCL design to improve the MEA structure and materials distribution in the CL [5-8],. They demonstrated that non-uniform CL structures can increase electrode performance compared to monolayer CLs, using the same catalyst and Pt loadings [9-13]. A non-uniform multilayer electrode proposed by Yoon et al. [5] improved oxygen reduction by developing a cathode structure with good proton and electron conduction properties composed of different Nafion ionomer (EW 1100) contents. Nafion ionomer contents in the first and second layers were varied from low (10 wt.%) to high (60 wt.%). The single cells adopting four variations of the double layered cathode designs showed a high pressure drop but demonstrated the best performance compared to single-layer cathodes. Roshandel et al. [14] conducted a study on multilayer cathodes for PEFCs showing that fuel cell performance can be significantly influenced by porosity variation in a gas diffusion layer (GDL). Xie et al. [6] designed GDEs containing gradient Nafion (5 wt. % in alcohols/water, Aldrich) distribution and found that cathode performance improved when Nafion content is higher in the GDE towards the CL/ membrane interface and lower towards the CL/carbon paper interface. Zhang & Shi [15] considered a GDE with dual bonded CL consisting of PTFE-bonded Pt/C on a microporous layer with ionomer-bonded Pt/C deposited on it. The dual bonded CL MEA had higher performance than conventional CL and increased energetic yield from 40%-50%. In 2008, Kim et al. [16] designed anode and cathode CLs with gradient Nafion® content (EW1100, 5 wt% solution, DuPont Inc.) and varied Pt loading. The dual catalyst layer coated MEA showed higher cell performance at the high current density region than the monolayer MEA design. Jung et al. [17] proposed an electrode composed of a highly phase-separated 1-methyl-2-pyrrolidinone (NMP)-based external layer and a lowly phase-separated glycerol-based inner layer. The proposed electrode resulted in increased cell performance in the high-current region. They later improved on their previous work [18] by lowering the Pt loading in the inner and outer layers to 0.16 and 0.04 mg_{Pt}/cm^2.The dual layer electrode had approximately 4 times larger current density at 0.6 V than monolayer CL MEAs.

Kim et al. [19] designed a double layer cathode with overall Pt loading fixed at 0.4 mg_{Pt}/cm^2, and different Pt loading ratios of inner and outer layers. The MEA with an inner layer of 0.3 mg_{Pt}/cm^2 and an outer layer of 0.1 mg_{Pt}/cm^2 cm^{-2} exhibited the best performance. This performance was better than that of the conventional single-layered electrode by 13.5% at a current density of 1.4 $A.cm^{-2}$. Chen et al. [20] developed a gradient design of Pt/C ratio and Nafion (5 wt. % solution, Du Pont, USA) content in PEMFC. They reported a higher power density for the optimal gradient design MEA which was 28.4% and 135.7% higher than the conventional single-layer CL MEA under high and low humidity, respectively. Shahgaldi et al. [8] designed a CCL with various gradients of ionomer distribution and this ionomer-gradient design improved Pt utilization by about 15% when compared with the conventional one-layer CCL design; and reduces resistances to both mass and proton transport as well.

While many studies have investigated the effect of stratification on performance [6], [8], [11], [13], [15-20], none of the studies have investigated the effect of stratification on MEA durability. This study will reduce the Pt loading of CCLs through ionomer graduation/stratification using ultrasonic spraying fabrication. Support corrosion in CCLs is a major contributor to the reduced stability and lifetimes of PEFC [21], and has remained relatively unexplored in gradient CCL designs. The structural degradation of MEAs due to carbon corrosion will therefore also be investigated to compare the durability of stratified and non-stratified CCLs.

2. Materials and Methods

2.1. MEA preparation

For both monolayer and stratified CCL MEAs, the catalyst ink was prepared using the same ink procedure. The catalyst ink was prepared by dispersing HySA-K40 (HyPlat) Pt on carbon (Pt/C) in 99.9 % isopropyl alcohol, deionized water, and Aquivion® ionomer (26 wt.% solids, D79-25BS Solvay, USA). The catalyst slurry was coated onto 50 cm^2 M820.15 gore membrane using the ultrasonic spray method. The ionomer content of the monolayer CCL design was 24 wt.%. For a stratified CCL design, two catalyst inks containing 24 wt.% and 28 wt.% ionomer contents were prepared. The first ink slurry containing 28 wt.% ionomer content was sprayed onto the membrane to form the first layer until a targeted Pt loading was reached as shown in Table 1. The second ink mixture, containing 24 wt% ionomer, was deposited onto the first layer of catalyst to form the outer layer (Table 1). The cathode Pt loading was 0.4 mg_{Pt}/cm^2 for the monolayer CCL and 0.35 mg_{Pt}/cm^2 for the stratified CCL MEA design. The anode Pt loading was fixed at 0.1 mg_{Pt}/cm^2 for both the monolayer and stratified MEA designs. After coating, the CCM was gasketed and hot-pressed at 90°C, 10 000 kPa for 1 min using a hot-press to ensure complete sealing. The gasketed CCM was sandwiched between two double-layer gas diffusion layer (GDL) (Avcarb MB30) to form an MEA. The MEA thickness was then measured using a thickness gauge.

Table 1. Specifications of monolayer and stratified CCL designs

	Cathode Pt loading (mg_{Pt}/cm^2)		**Overall Cathode Pt loading (mg_{Pt}/cm^2)**	**Ionomer loading (wt.%)**	
	Inner layer	**Outer layer**		**Inner layer**	**Outer layer**
MEA #1	0.40	-	0.40	24	-
MEA #2	0.35	-	0.35	24	-
MEA #3	0.050	0.30	0.35	28	24
MEA #4	0.10	0.25	0.35	28	24
MEA #5	0.15	0.20	0.35	28	24
MEA #6	0.20	0.15	0.35	28	24

2.2. Physical characterization techniques

The Brunauer-Emmett-Teller (BET) technique and scanning electron microscopy (SEM) analysis were used to characterize the MEAs. SEM was performed using an FEI Nova NanoSEM 230. The SEM images were taken using a backscatter detector in 2000, 5000 & 10 000 x magnification, and 20.0 keV. BET analysis was performed using a Micrometrics TriStar II 3020, to determine the surface area, pore size, and cumulative pore volume of the CLs. During BET analysis, the sample was cooled to liquid nitrogen temperature, followed by physical absorption (based on van der Waals interactions) of N_2 molecules from a known amount of gas onto the surface of the sample. The surface area was measured by exposing nitrogen to the surface of the solid and by calculating the amount of adsorbate gas corresponding to the monomolecular layer on the surface.

2.3. Electrochemical measurement

The MEA was placed into a 50 cm^2 single cell fuel cell hardware consisting of two graphite bipolar plates with parallel flow field channels, current collectors and two end plates. The assembly was compressed to a torque of 5 N.m.

All single cell tests were conducted with a fully automated FuelCon fuel cell test station in the humidity range of 20 - 100 % RH. The MEA was conditioned prior to polarization measurements: the cell was heated up to 80 °C at 100 % RH, with hydrogen and airflow in the potential range between 0.3 V and 1 V with 0.05 V steps. Pure H_2 gas was supplied at 1.11 Nl/min to the anode and Air at 2.65 Nl/min to the cathode compartment. The conditioning cycle was repeated 12 times for a 2-hr period. The single cell was activated at 0.3 V using hydrogen and air at 80 % relative humidity (RH), 74.6 °C operating temperature and 2 bar back pressure for both anode and cathode. Polarization curves (IV) were measured at 80 °C when the cathode and anode were fed with air and pure hydrogen with stoichiometries of 2.5 and 1.5, respectively. I-V curves at 20 RH%, 60 % RH and 20 RH%, at both electrodes, were recorded. The cyclic voltammograms (CVs) were collected under gas fluxes of 500 mL/min N_2 at the cathode and 300 mL/min H_2 at the anode at 80 °C from 20 – 100 % RH. The potential scan range in the CV was 0.04 – 0.9 V scanned at 50 mV/s. The hydrogen adsorption peak was then used to determine the electrochemical surface area (ECSA). The EIS was measured in a frequency range from 20 kHz to 100 mHz with an amplitude of 5 mV while the cell was operated at 500 mA/cm^2 and 80 °C.

2.4. Carbon corrosion test

An accelerated stress test (AST) inducing carbon corrosion and severe degradation of the MEA was conducted. The cell was first conditioned at the standard conditions listed in Table 2.

Table 2. Operating conditions for the standard fuel cell operation and carbon corrosion AST.

	Cell temperature (°C)	**Gas flow rates (Nl/min)**	**Feed gas temperature (°C)**	**Back pressures (bar)**	**RH (%)**
Standard operating conditions	80	1.11 H_2 (anode) 2.65 Air (cathode)	50℃ anode (H_2) 50℃ cathode (Air)	2	100 (anode) 80 (cathode)
Carbon corrosion test conditions	80	0.2 H_2 (anode) 30 N_2 (cathode)	83℃ anode (H_2) 83℃ cathode (N_2)	1	100 (anode) 100 (cathode)

During the carbon corrosion test, carbon and water oxidation are incurred by cycling voltage across the MEA. The potential was cycled repeatedly between 0 and 1.2 V at 50 mv/s. The process was repeated for up to 6000 cycles. The experimental cycles were divided into the following segments: initial state, 20 cycles, 180 cycles, 200 cycles, 600 cycles, 1000 cycles, 2000 cycles, and 6000 cycles. Polarization curve, hydrogen crossover, and CV were measured in each segment.

3. Results and Discussion

3.1. Reducing Pt loadings in stratified MEAs

The loading in the CCL was reduced to 0.35 mg_{Pt}/cm^2 in a monolayer as well as stratified configurations. The thicknesses of the MEAs are presented in Table 3. The reduced Pt loading MEAs (MEA #2 -#6) were 16 - 40 % thinner than the high Pt loading monolayer MEA #1, mostly due to decreased Pt loading. Increasing ionomer loading in the CL increases Pt/C-ionomer agglomerate size. Consequently, the stratified CCLs had different

Pt/C-ionomer agglomerates due to their varying Pt/C to ionomer ratios- MEAs with more 28 wt.% I loading (MEA #5 & #6) were thinner than those with more 24 wt.% I (MEA #3 & #4). It is likely that the agglomerates of the 28wt% ionomer content MEAs were closely packed together and yielded a dense, thin CL structure.

Table 3. The thickness and pore characteristics of the monolayer and stratified CCL MEAs.

	Thickness (mm)	Bulk density (g/cm³)	Cumulative pore volume (cm³/g))	BET surface area (m²/g)	% Porosity
MEA #1	0.05180	0.8157	0.1443	70.18	11.77
MEA #2	0.03067	1.413	0.2331	70.43	32.94
MEA #3	0.04200	1.002	0.09620	67.27	9.640
MEA #4	0.04330	0.9566	0.1867	57.77	17.89
MEA #5	0.03700	1.141	0.04209	54.50	4.800
MEA #6	0.03800	1.111	0.09623	47.22	10.68

Although MEA #1 and #2 had the same ionomer loading, MEA #2 had a significantly larger porosity than MEA #1 because of its decreased Pt loading. Decreasing the Pt loading causes the void fraction and solid ionomer contact to decrease [11], and therefore increases the surface area. Stratified MEAs had a lower BET surface area than monolayer MEAs due to the presence of 28 wt.% I layer as well as a layer interface. Increasing ionomer content increases ionomer coverage in the CL and thus decreases the surface area. The BET surface area of the stratified MEAs decreased with increasing thickness of the first layer containing 28wt% ionomer or with decreasing thickness of the second layer containing 24wt% ionomer. This can be correlated to the size of agglomerates present in the CL. Pt/C-I agglomerate size increases with ionomer content. Therefore, increasing 28 wt.% ionomer thickness causes larger agglomerates to be formed, subsequently decreasing the surface area in the CL.

3.1.1. Electrochemical surface area

Figure 1 presents the ECSAs of the stratified and non-stratified MEAs at full and 12% reduced Pt loading.

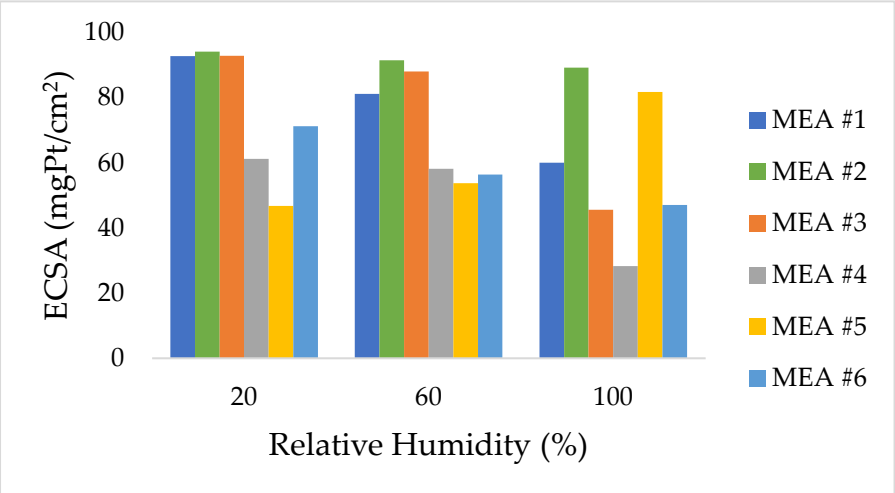

Figure 1. The ECSAs for the stratified and non-stratified MEAs determined at 20- 100 % RH.

The monolayer MEA #2 with reduced Pt loading, demonstrated the largest and most consistent ECSAs under all RH conditions, owing to its highly porous agglomerate structure

which exposed Pt active sites. For similar reasons, the stratified CCL MEA with the largest BET surface area and more 24 wt.% I loading (MEA #3) demonstrated larger ECSAs from 20-60 % RH conditions. The ECSA of the stratified MEAs decreased with increasing thickness of the first layer. This is likely due to higher ionomer coverage also shown with decreasing BET surface area. However, at 100 % RH the ECSA was significantly larger for the low porosity MEA #5 compared to other stratified MEAs. The increase of ECSA with RH was also reported by Fan et al. [22] who mainly attributed this trend to the improved contact area between Pt particles and water domains instead of the formation of new transport paths. The low porosity and denser agglomerate structure of MEA #5 could have played a role in increasing the contact area between water domains and ionomer/catalyst aggregates.

3.1.2. MEA performance

To determine the effect of ionomer stratified layers on the electrochemical performance of the resulting MEA, the polarization curves are compared in Figure 2.

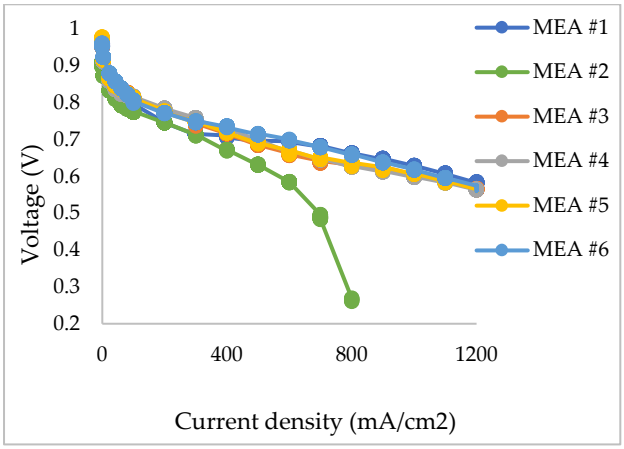

(**a**)

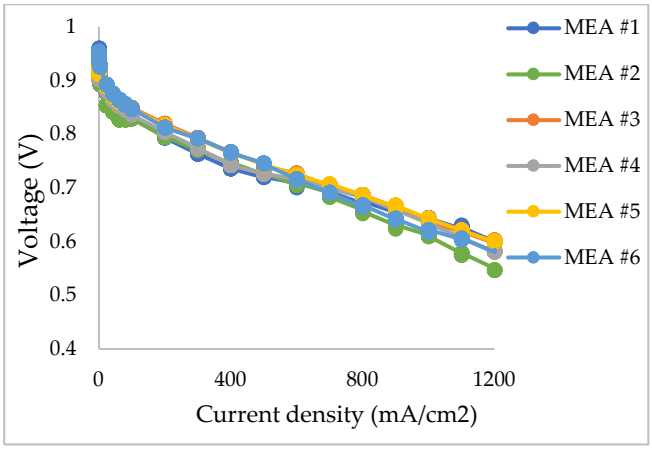

(**b**)

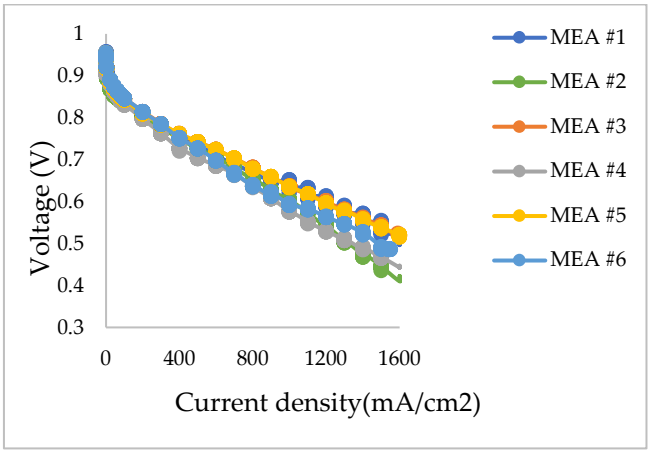

(c)

Figure 2. Polarization curves for monolayer and stratified MEAs obtained for: (a) 20 % RH; (b) 60 % RH; (c) 100 % RH.

The stratified CCL MEAs performed better than the loading equivalent monolayer MEA #2. This performance improvement is attributed to the effect of the higher ionomer loading in the first layer which increased proton conductivity; and a lower

ionomer loading in the second layer which reduced mass transport losses [8], [11]. At low current densities (200 mA/cm² and lower), the activation losses of monolayer MEA #2 were higher than the stratified MEAs. At dry conditions, the performance of stratified MEAs improved with increasing thickness of the 28 wt.% layer. MEA #6, which had the thickest 28 wt.% I layer, demonstrated superior performance owing to its higher proton conductivity. MEA #3 and #5 performed better than MEA #4 and #6 under all studied RH conditions which could be related to their I/C ratio. From medium to high current densities, the voltage drop was greater for MEA #2 under all RH conditions due to increased ionic transport resistances, which limited its performance. At high current densities, MEA #4 and #6 experienced higher voltage losses. These MEAs do not have an optimized I/C ratio for optimal ionic and water transport. Figure 3 compares the performances of the lower Pt loading MEAs (MEA #2-#6) determined at 0.65V with the benchmark MEA #1 with 0.4 mg_{Pt}/cm^2 Pt loading.

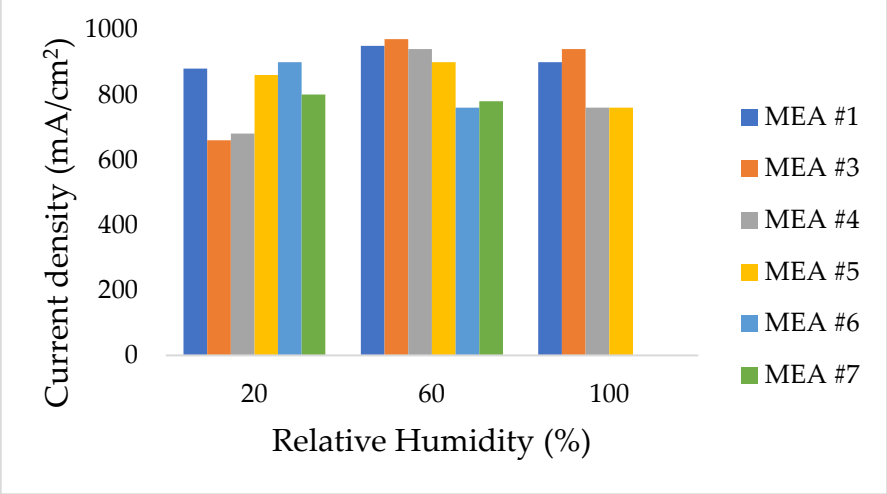

Figure 3. The current density (mA/cm²) for the stratified and non-stratified MEAs determined at 20- 100 % RH determined at 0.65 V.

At dry conditions, MEA #2 demonstrated very low performance, only achieving 52.27 % of MEA #1's performance. The Pt utilization may have dropped significantly for the low Pt content 24 wt.% MEA because the I/C ratio deviates from the optimum value. The performance of the stratified MEAs decreased with a decrease in the first layer thickness. Higher ionomer loading is crucial for decreasing ionic resistances at dry conditions. When the RH is increased, the ionomer absorbs moisture and elongate ionic paths. Higher ionomer loading means more hydrophilic zones and greater ionomer swelling, which increases charge transfer resistances at higher RH. As a result, when the RH increased, MEAs with more 24 wt.% I loading became favorable as they demonstrated better performance. Generally, the performance of the reduced Pt loading MEAs was comparable to the benchmark monolayer MEA #1. The performance data shows that it is possible to reduce Pt loading by 12% and still achieve similar benchmark performance under various RH conditions. Sasikumar et al. [24] studied the dependence of ionomer content on Pt loading and it was found that that the optimal ionomer content depends on the Pt loading. This study confirmed that the performance depends on the I/C loading ratio. The MEA with Pt ratio= 1:6 (0.05 1st layer and 0.3 2nd layer) gave the best performance at higher RH and the one with 1:0.75 (0.15 1st layer and 0.2 2nd layer) ratio performed best at dry conditions.

3.1.3. EIS analysis

To further understand the performance of the reduced Pt loading MEAs (MEA #2 - #6), EIS was used to determine the key resistances. The corresponding EIS analysis was performed at 0.5 mA/cm² current density in a H_2/Air and a frequency sweep from 20 kHz – 0.1 Hz at steps of 50. The resulting Nyquist plots are presented in Figure 4 showing the imaginary impedance (Z'') as a function of real impedance (Z'). The plots highlight the impedance spectrum from 20 kHz- 0.1 Hz with an arc evident within a frequency range. The mass transfer resistance arc was reasonably small to insignificant in the Nyquist plots because the study was conducted at low current density (0.5 mA/cm2) where charge transfer resistances dominate. The magnitude of the charge transfer arcs decreased with an increase in RH for all MEAs. At 100 % RH, the smallest arcs were demonstrated by the monolayer MEAs which signifies lower charge transfer resistances. Meanwhile, ohmic resistances decreased with increasing RH for all MEAs.

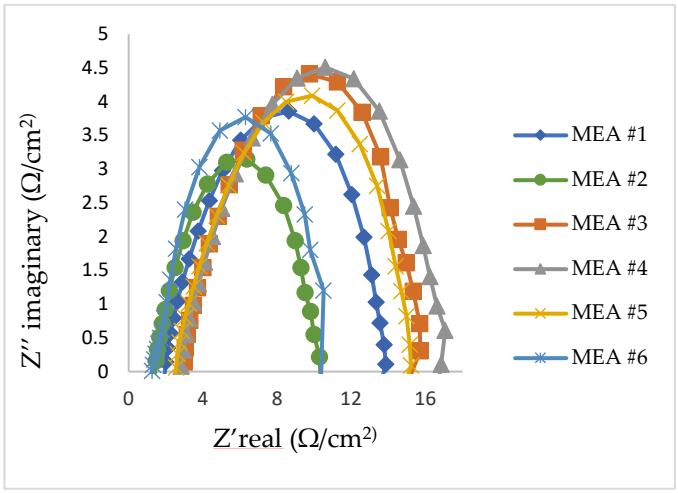

(**a**)

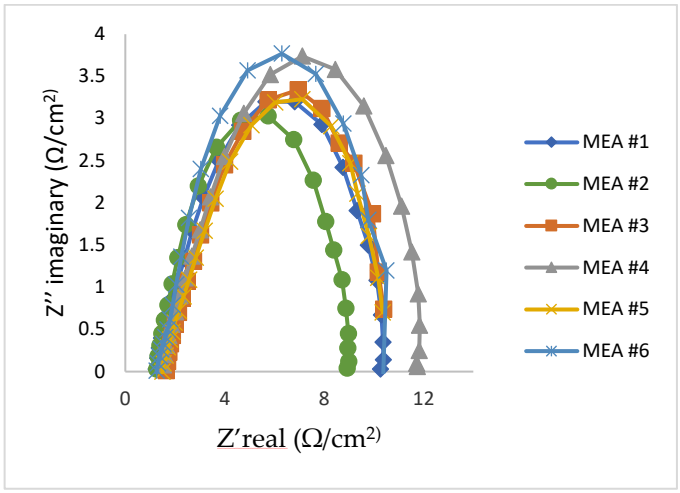

(**b**)

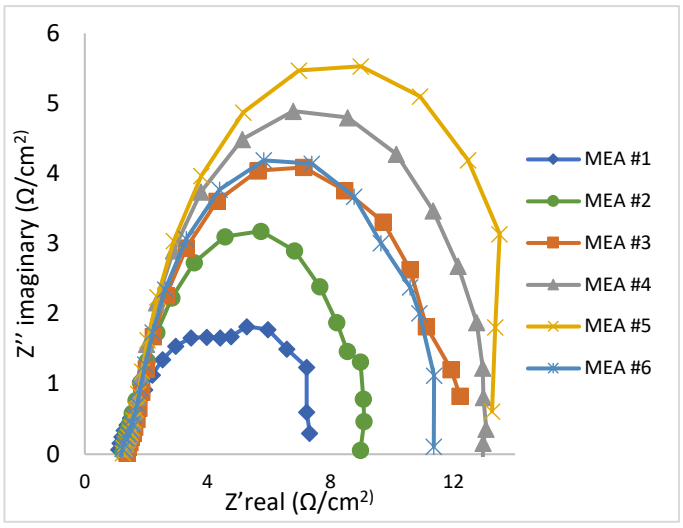

(**c**)

Figure 4. Nyquist plots of benchmark monolayer MEA (MEA #1) and reduced Pt loading MEAs (MEA #2- #6), under: (a) 20 %; (b) 60 %; (c) 100 % RH.

The Nyquist plots were fitted with a Randles equivalent circuit model [24] and the results are shown in Table 4. R1 is the ohmic resistance and the diameter of the Nyquist plot semi-circle (charge transfer resistances) is represented by R2.

Table 4. The EIS fitting parameters obtained from the Randles equivalent circuit model.

		MEA #1	MEA #2	MEA #3	MEA#4	MEA #5	MEA #6
R1 (Ωcm^2)	20 % RH	2.019	1.759	2.748	2.854	2.683	1.328
	60 % RH	1.325	1.600	1.655	1.560	1.253	1.263
	100 % RH	1.115	1.560	1.438	1.334	1.320	1.336
R2 (Ωcm^2)	20 % RH	10.56	8.157	9.004	8.561	8.090	7.146
	60 % RH	5.873	6.278	6.712	6.503	7.274	7.339
	100 % RH	6.004	6.228	7.565	7.788	7.339	7.177

At 20 % RH, the ohmic and charge transfer resistances both increased substantially for all MEAs due to low water content in the membrane, consequently decreasing performance. Stratified MEAs demonstrated lower charge transfer resistances compared to the 0.4 mg_{Pt}/cm^2 monolayer MEAs (MEA #1) due to increased ionomer loading in the first layer. In stratified MEAs, charge transfer and ohmic resistances both decreased with increasing ionomer thickness of the first layer. Increasing the thickness of the first layer increased proton conductivity and thus reduced ohmic resistances. The lowest charge transfer and ohmic resistances 7.146 Ωcm^2 and 1.328 Ωcm^2 were demonstrated by MEA #6 respectively, which confirmed the better performance of this MEA at dry conditions. Hence, increasing the thickness of 28 wt.% I in the first layer of stratified CCL MEA is beneficial for increasing performance at dry conditions.

At 60 % RH, charge transfer resistances decreased with an increasing 24 wt.% I layer thickness in stratified MEAs. This can be attributed to the effect of ionomer swelling which increases with ionomer thickness and RH covering electrochemical conductive areas and elongating charge transfer pathways in the high ionomer loading stratified MEAs [26-27]. Similarly, monolayer MEAs, which had the least ionomer loading, had the smallest charge transfer resistances at fully humidified conditions. From 60-100 % RH, charge transfer and ohmic resistances were significantly lower for the benchmark MEA #1 because it had a higher Pt loading which increased ORR kinetics. MEA #2 exhibited larger ohmic resistances under all RH conditions contributing to its poor performance. This means that the 24 wt.% I loading is not sufficient for 0.35 mg_{Pt}/cm^2 loading; a higher ionomer loading is required.

3.2. *Durability comparison of stratified and monolayer MEAs*

While the reduced Pt loading stratified CCL MEAs performed better than the monolayer equivalent MEA #2, the durability of these stratified MEAs needs to be established. Therefore, a carbon degradation test was performed to compare the durability of the reduced Pt loading stratified MEA with monolayer MEA #1. MEA #6, which was more consistent in reaching performance targets under the studied RH conditions, was selected for the degradation test. Cyclic voltammetry, SEM, and polarization analysis were performed to determine the MEA durability during potential cycling. During this AST, carbon and water oxidation are incurred by cycling voltage across the MEA.

3.2.1. Catalyst layer degradation

The cross-sectional images of the stratified and monolayer CCL MEAs before and after the degradation test in the respective MEAs after the 30-h AST are shown in the SEM images of Figure 5. The MEAs used for SEM imaging before and after AST were not the same due to the nature of SEM sample preparation. The CL thicknesses may therefore vary because of inconsistencies during manufacturing inherent to the production process, and therefore only serve as an estimation of catalyst layer integrity after the AST.

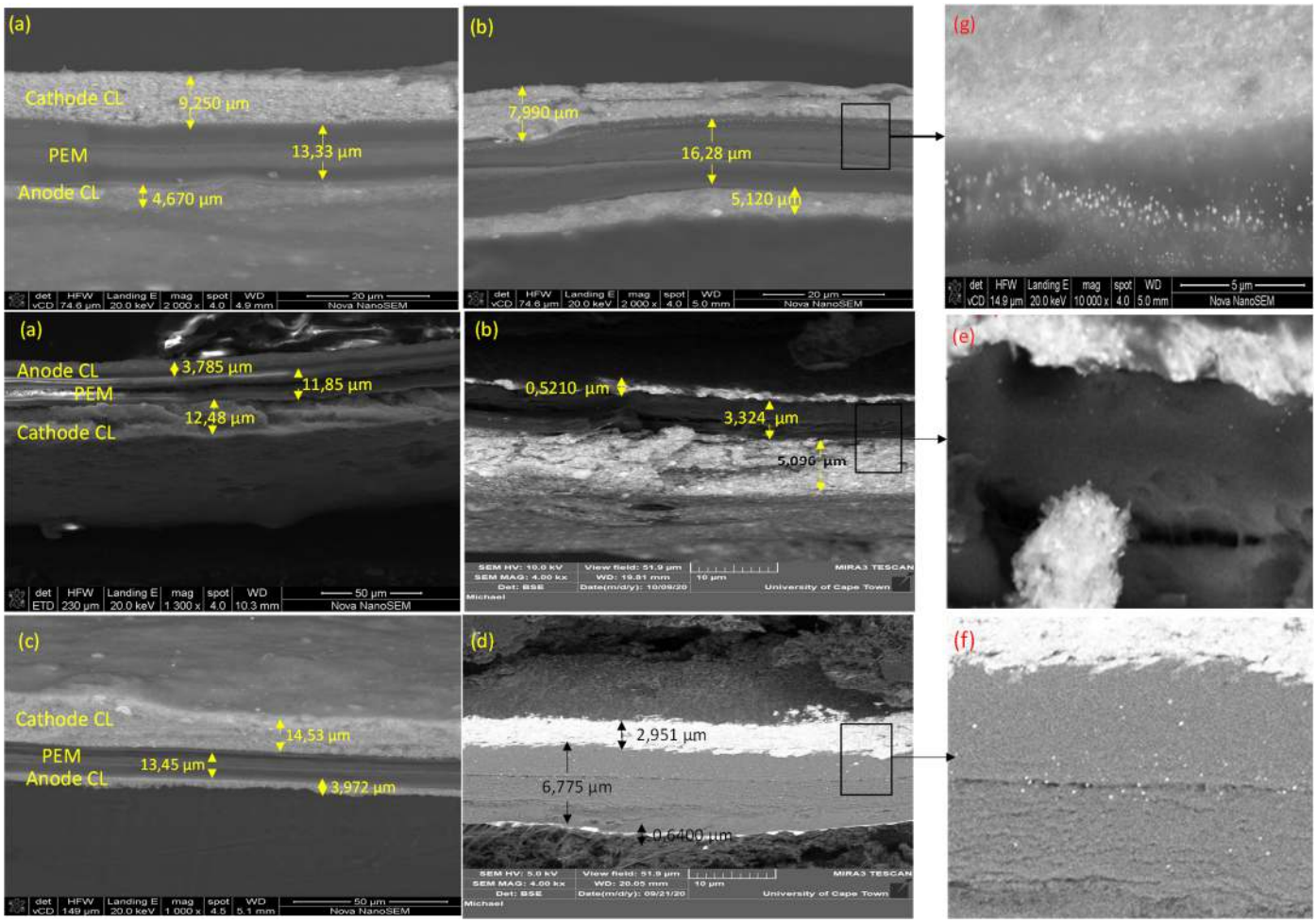

Figure 5. A cross-sectional image of an unused: (a) monolayer CCL MEA #1; (c) monolayer CCL MEA #2; (e) CCL stratified MEA#6. After the carbon corrosion test, the SEM images of the degraded: (c) MEA #6; (d) MEA #2, were captured. A magnified image of the degraded: (g) MEA #1; (h) MEA #2; (i) MEA #6, showing Pt migrated from the CL into the PEM.

The CCL of the unused MEA #1 is thicker than MEA #2 and #6 because it has a higher Pt loading. MEA #6 CCL is also 19.29 % thicker than MEA #2 before the degradation test, owing to the thick 28wt% ionomer layer on the inner layer of MEA #6. Figure 5 (b), (d), and (f) show a thinner CL structure of MEA #1, #2, and #6 which verifies collapsing of the CL structure because of severe carbon degradation. The MEA thicknesses are summarized in Table 5.

Table 5. The thicknesses of MEAs before and after the carbon degradation test.

	MEA Components	Thickness before degradation (µm)	Thickness after degradation (µm)
MEA #1	CCL	17.49	7.990

	PEM	13.86	16.28
	ACL	5.210	5.120
MEA #2	CCL	12.48	5.029
	PEM	11.85	3.324
	ACL	3.875	0.521
MEA #3	CCL	14.53	2.951
	PEM	13.47	6.785
	ACL	3.972	0.6400

After the carbon degradation test, the thinning of both the anode and cathode CLs due to carbon support oxidation was observed for all MEAs. The anode CL thinned by 83.88 % for the stratified MEA and 86.55 % for the reduced Pt loading monolayer MEA#2. There was no significant change in the anode thickness of MEA #1 (1.72 %) over the degradation period. The CCL thickness of MEA#1 was reduced by 54,32 %; lower Pt loading monolayer MEA#2 was reduced by 79.69 % and stratified CCL MEA#5 by 59.16 %. The Pt/C, ionomer, and membrane together comprise the mechanical strength of a CCM. Decreasing any of these materials decreases the mechanical strength of an MEA. The degradation of the CLs and membrane was greater for the reduced Pt loading MEAs compared to the higher Pt loading MEAs. After electrochemical carbon degradation MEA #2 and MEA #6 experienced membrane dehydration/thinning while higher Pt loading MEA #1 experienced membrane swelling. In the high Pt loading monolayer MEA #1 the PEM expands during the carbon corrosion test due to isotropic and anisotropic swelling [28]. This indicates high water retention MEA #1 as thicker CLs retain more water. The water content in the membrane imposes swelling/hydration and results in high mechanical stresses in the membrane which could lead to membrane failure and gas cross over [29-31]. Thinning of the PEM membrane observed for lower Pt loading MEAs resulted from thermal and chemical degradation of the membrane during the carbon degradation process and it can lead to both gas crossover and electrical shortening [32-34]. PEM thickness decreased by 49.61 % for MEA #6 and 71.93 % for MEA #2. Sethruman et al. [33] showed that inadequate water content and high temperature accelerate membrane thinning. Therefore, the high ionomer loading adjacent to the membrane of the stratified MEA #6 played a role in reducing PEM degradation by retaining moisture closer to the PEM and improving heat dissipation.

Pt migration was also observed for all MEAs, but it was less for MEA #2 (Figure 11 (h)) compared to MEA#1 (Figure (g)) and MEA #6 (Figure 11 (i)). Pt aggregates can be observed as white particles on the PEM shown in Figure 5 (g) and (i) which suggests that Pt detached from the carbon support due to corrosion. As the carbon support degrades, Pt particles dissolve and migrate and precipitate onto the membrane surface resulting in loss of electrochemical activity in the CL. Pt in the membrane is electronically and ionically isolated and cannot be accessed by gas reactants which leads to electrical performance degradation [21], [34].

3.2.2. ECSA loss

The loss of Pt was evaluated periodically during the carbon degradation test, to examine the effect of electrochemical carbon corrosion on the ECSA. To compare the ECSA losses obtained in each MEA with progressive cycling, the ECSA losses were normalized to its beginning-of-life (BoL) ECSA and the following equation was used:

$$\%\, ECSA\ loss = \frac{ECSA_{BoL} - ECSA_{n-th\ cycle}}{ECSA_{BoL}} x\ 100, \quad (1)$$

Where ECSA BoL is the ECSA at the beginning of life, and ECSAn-th cycle is the measured ECSA after the n-th cycle. The comparison of ECSA in Figure 6 shows a decrease in ECSA for all MEAs with progressive cycling.

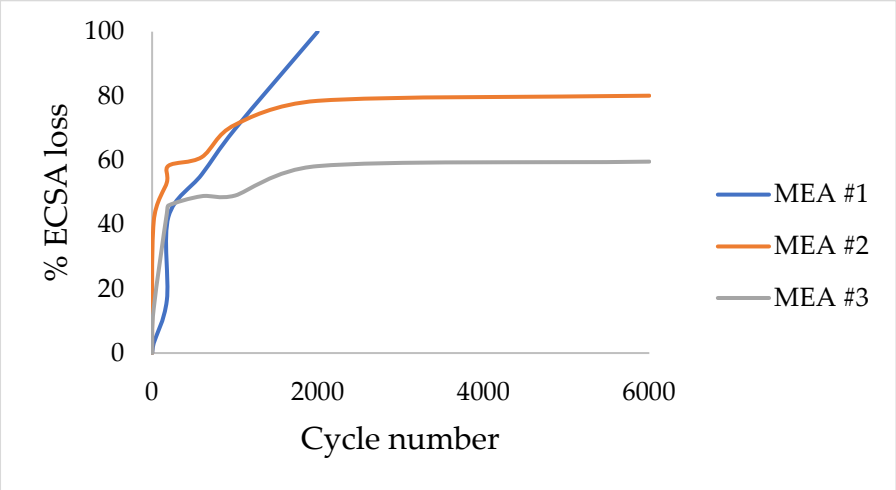

Figure 6. ECSA loss during cycling of the stratified MEA #6 and monolayer MEAs, MEA #2 and MEA#1.

The ECSA decreased over the degradation period due to carbon support corrosion and Pt dissolution. During electrochemical carbon corrosion, carbon is converted to CO_2 gas. As a result of the reduced carbon support area, Pt particles agglomerate or dislodge, leading to a decrease in Pt surface area [35]. There was accelerated decay in the ECSA of high Pt loading MEA #1 compared to lower Pt loading MEA #2 and #6 congruent with the results reported by Speder et al. [36]. This could be due to the extensive loss of Pt resulting from extensive Pt dissolution as observed in Figure 5 (g). MEA#1 reached a 100 % ECSA loss after only 2000 cycles while MEA #2 had a total loss of 80 % after 6000 cycles and only 59 % total ECSA loss for MEA #6. Although it appears in Figures 5 (i) and (h) that MEA #6 experienced more Pt dissolution and CCL disintegration than MEA #2, the ECSA of MEA #2 decreased significantly faster than MEA #6. The extensive loss of ECSA in MEA #2 resulted from a drastic PEM degradation as observed in Figure 5 (d), which possibly increased hydrogen crossover [37].

3.2.3. Decrease in electrochemical performance

Polarization curves were performed with 59 % RH on both anode and cathode, at periodic intervals during the degradation period. Figure 7 shows the performance curves of the stratified MEA #6 and the monolayer MEAs over the degradation period.

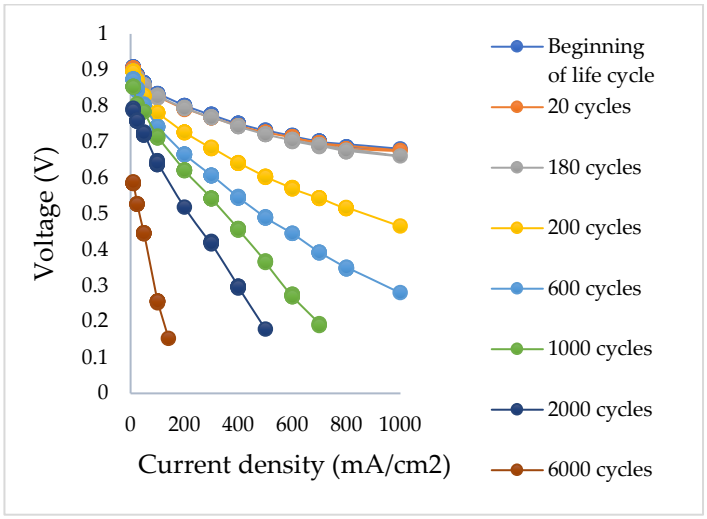

(**a**)

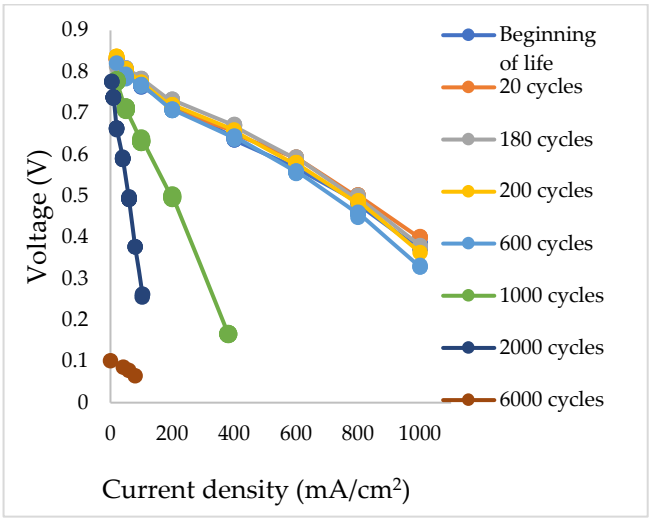

(**b**)

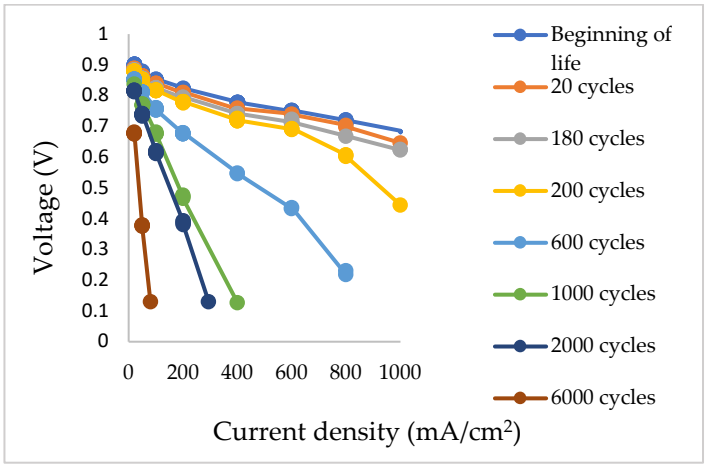

(**c**)

Figure 7. Performance curves taken during potential cycling for a: (a) high Pt loading monolayer MEA #1; (b) reduced Pt loading monolayer MEA #2; (c) Stratified CCL MEA #6.

The performance curves show a decrease in cell potential after every following potential cycling period. The initial performance of the MEAs is comparable but their performance degradation is distinctive. The output voltage decreased from the low to the high current density region with progressive cycling due to CL morphology changes caused by carbon degradation, mainly ECSA loss due to particle agglomeration and CL thinning. Carbon degradation and CL thinning reduce electron conduction in the Pt/C phase, contributing to ohmic losses while PEM degradation leads to proton conductivity losses- increasing ionic transport resistances and limiting performance. Besides, CL surface roughening due to carbon corrosion makes the CL hydrophilic and adds oxides groups resulting in oxygen diffusion and water management challenges, which drastically affects performance [38-39].

The OCV of MEA #2 drastically decreased after 6000 cycles from 0.83-0.101 V whereas MEA #6 OCV decreased from 0.910-0.680 V and MEA #1 from 0.89-0.585 V. These OCV losses can be correlated to increased hydrogen cross overs with membrane swelling/thinning [37], [40] and Pt surface area losses during potential cycling.

To compare the performance losses obtained in each MEA, the voltage losses were normalized to its beginning-of-life (BoL) cell voltage and the following equation was used [41]:

$$\%\ Performance\ loss = \frac{V_{BoL} - V_{n-th\ cycle}}{V_{BoL}}\ x\ 100, \quad (2)$$

Where VBoL is the cell voltage at Beginning of life, and Vn-th cycle is the voltage after the n-th cycle. Figure 8 presents the percentage performance loss of each MEA versus the cycling period measured at 200 mA/cm^2.

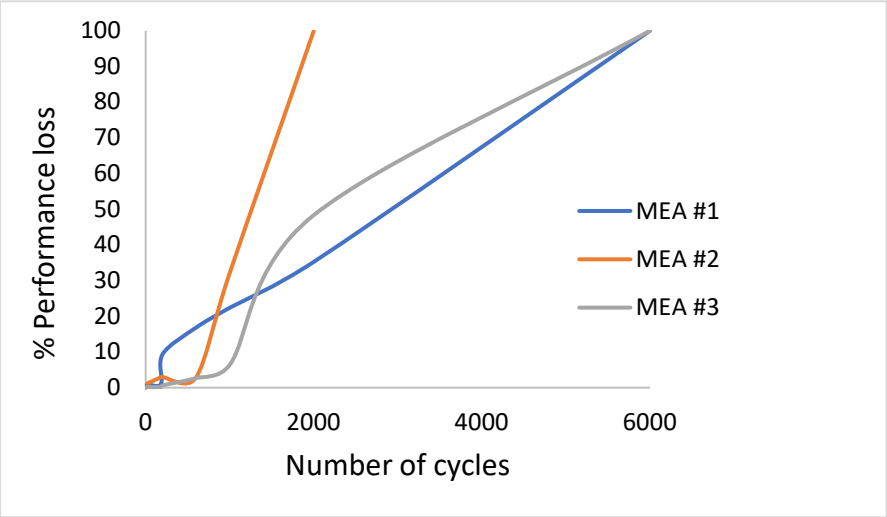

Figure 8. Percentage performance loss of MEAs during potential cycling, measured at 200 mA/cm2.

Performance loss begins to increase sharply after 1000 cycles for all MEAs. Higher Pt loading MEA #1 experienced lower activation losses compared to the reduced Pt loading MEAs. At 2000 cycles, MEA #2 had already reached a 100 % performance loss while MEA #6 demonstrated 54 % loss and MEA #1 35 % loss.

Performance degradation was substantial for both the monolayer and stratified CCL MEAs, but the degradation of the CL after prolonged corrosion was slower in the MEA with stratified CCL. This was corroborated by higher ECSA; lower kinetic, and OCV losses after carbon degradation. The high ionomer coverage in the first layer of MEA #6 may have reduced carbon corrosion by retaining moisture closer to the membrane, preventing severe membrane dryness which causes PEM degradation. The bilayer interface also played a role in enhancing the durability of the MEA by disrupting the rate of mass transport during carbon degradation test, reducing the carbon corrosion rate.

4. Conclusions

Using an ionomer-gradient approach, stratified CCL MEAs were designed for low-temperature PEFC. The goal of the project was to reduce Pt loading in the stratified layers without sacrificing performance and lifetime. This study has shown that using ionomer stratification to decrease the Pt loading in an MEA yields better performance compared to the monolayer MEA equivalent. Compared to the benchmark MEA at 0.4 mg$_{Pt}$/cm^2, reduced Pt loading stratified MEA showed ±2 % performance change from 20- 60 % RH and about 13 % performance increase at fully humidified conditions. This is in stark contrast to a 13% to 47.72 % decrease in performance observed of the reduced Pt monolayer MEA compared to the commercial benchmark. Not only did the reduced Pt loading stratified

MEA perform better than the reduced Pt loading monolayer MEA, but it also proved to be more durable.

The AST for all the MEAs saw a decrease in performance which was correlated to a decrease in CCL thickness, membrane degradation, and ECSA loss. Stratified MEAs were shown to be more durable than monolayer MEAs at equivalent Pt loadings. The high ionomer loading adjacent to the membrane of the stratified MEAs increases moisture in the CL, thus lowering the degradation process of the stratified CCLs. The bilayer interface in the stratified CCL MEA also played a role in disrupting mass transport during the fuel starvation process. Compared to the benchmark high Pt loading MEA, the stratified MEA increased the durability of an MEA by decreasing the ECSA loss by 41.83 % and OCV losses by 26.25 %. However, a slight increase of 18.82 % in kinetic losses was observed. These findings are anticipated to contribute to the development of more durable MEAs for low-temperature PEFCs.

Funding: This research was funded by National Research Foundation (NRF) Free Standing Innovation grant and HySA Catalysis funded by the South African Department of Science and Technology.

Acknowledgments: Special thanks to HyPlat (Pty) Ltd. for providing all materials used for experiments in this study.

Conflicts of Interest: The funders had no role in the design of the study; in the collection, analyses, or interpretation of data; in the writing of the manuscript, or in the decision to publish the results.

References

1. Fan, L., *Development and Characterisation of functional composite materials for advanced energy conversion technologies.* Royal Institute of Technology: Stockholm, 2013.
2. Zhang, J., In *PEM Fuel Cell Electrocatalysts and Catalyst Layers*, Zhang, J., Ed. Springer Science & Business Media: Vancouver, Canada, 2008; pp 1-78.
3. Ye, S.; Banham, D., Current Status and Future Development of Catalyst Materials and Catalyst Layers for Proton Exchange Membrane Fuel Cells: An Industrial Perspective. *ACS Energy Letters* **2017**, 1-8.
4. Gasteiger, H. A.; Panels, J. E.; Yan, S. G., Dependence of PEM fuel cell performance on catalyst loading. *J Power Sources* **2004,** *127* (1-2), 162–171.
5. Yoon, Y.-G.; Yang, T.-H.; Park, G.-G.; Lee, W.-Y.; Kim, C.-S., A multi-layer structured cathode for the PEMFC. *J Power Sources* **2003,** *118* (1-2), 189-192.
6. Xie, Z.; Navessin, T.; Ken Shi, K.; Chow, R.; Wang, Q.; Song, D.; Andreausa, B.; Michael Eikerlinga, M.; Liua, Z.; Steven Holdcrofta, S., Functionally Graded Cathode Catalyst Layers for Polymer Electrolyte Fuel Cells II. Experimental Study of the Effect of Nafion Distribution. *J Electrochem Society* **2005,** *152* (6), A1171-A1179.
7. Su, H.-N.; Liao, S.-J.; Wu, Y.-N., Significant improvement in cathode performance for proton exchange membrane fuel cell by novel double catalyst layer design. *J Power Sources* **2010,** *195* (11), 3477–3480.
8. Shahgaldi, S.; Ozden, A.; Li, X.; Hamdullahpur, F., Cathode catalyst layer design with gradients of ionomer distribution for proton exchange membrane fuel cells. *Energy Convers Manage* **2018,** *171*, 1476-1486.
9. Wang, Q.; Eikerling, M.; Song, D.; Liu, Z., Structure and performance of different types of agglomerates in cathode catalyst layers of PEM fuel cells. *J Electroanal Chem* **2004,** *573*, 61-69.
10. Sun, W.; Peppley, B. A.; Karan, K., An improved two-dimensional agglomerate cathode model to study the influence of catalyst layer structural parameters. *Electrochimica Acta* **2005,** *50*, 3359–3374.
11. Srinivasarao, M.; Bhattacharyya, D.; Rengaswamy, R.; Narasimhan, S., Performance analysis of a PEM fuel cell cathode with multiple catalyst layers. *Int J Hydrogen Energy* **2010,** *35*, 6356-6365.

12. Song, D.; Wang, Q.; Liu, Z.; Navessin, T.; Eikerling, M.; Holdcroft, S., Numerical optimization study of the catalyst layer of PEM fuel cell cathode. *J Power Sources* **2004,** *126* (1-2), 104-111.
13. Cetinbas, F. C.; Advani, S. G.; Prasad, A. K., Optimization of polymer electrolyte membrane fuel cell catalyst layer with bidirectionally-graded composition. *Electrochim Acta* **2015,** *174*, 787-798.
14. Roshandel, R.; Farhanieha, B.; Saievar-Iranizad, E., The effects of porosity distribution variation on PEM fuel cell performance. *Renewable Energy* **2005,** *30* (10), 1557-1572.
15. Zhang, X.; Shi, P., Dual-bonded catalyst layer structure for PEMFC. *Electrochem Commun* **2006,** *8*, 1129-1234.
16. Kim, K.-H.; Kim, H.-J.; Lee, K.-Y.; Jang, J. H.; Lee, S.-Y.; Cho, E.; Oh, I.-H.; Lim, T.-H., Effect of Nafion gradient in dual catalyst layer on proton exchange membrane fuel cell performance. *Int J Hydrogen Energy* **2008,** *33* (11), 2783-2789.
17. Jung, C.; Vahc, Z. Y.; Kim, T.; Yi, S., Investigation of the dual-layered electrode composed of catalyst layers with different phase separation levels for PEMFC. *Electrochemica Acta* **2014,** *196*, 495-502.
18. Jung, C. Y.; Kim, S. K.; Lee, S. J.; Yi, S. C., Three-dimensional reconstruction of coarse dense catalyst layer for proton exchange membrane fuel cells. *Electrochemica Acta* **2016,** *211*, 142-147.
19. Kim, G. H.; Eom, K. S.; Kim, M. J.; Yoo, S. J.; Jang, J. H.; Kim, H.-J.; Cho, A. E., Design of an Advanced Membrane Electrode Assembly Employing a Double-Layered Cathode for a PEM Fuel Cell. *ACS Applied Materials & Interfaces* **2015,** *7* (50), 27581–27585.
20. Chen, G.; Wang, C.; Lei, Y.; Zhang, J.; Mao, Z.; Mao, Z. Q.; Guo, J.-W.; Li, J.; Ouyang, M., Gradient design of Pt/C ratio and Nafion content in cathode catalyst layer of PEMFCs. *Int J Hydrogen Energy* **2017,** *42*, 29960-299652.
21. Yu, X.; Ye, S., Recent advance and durability advancement of Pt/C catalytic cathode in PEMFC Part II: Degradation mechanism and durability enhancement of carbon supported platinum catalyst. *J Power Sources* **2007,** *172*, 145-154.
22. Fan, L.; Wu, K.; Tongsh, C.; Zhu, M.; Xie, X.; Jiao, K., Mechanism of Water Content on the Electrochemical Surface Area of the Catalyst Layer in the Proton Exchange Membrane Fuel Cell. *J Phys Chem Lett* **2019**, 6409–6413.
23. Sasikumar, G.; Ihm, J. W.; Ryu, H., Optimum Nafion content in PEM fuel cell electrodes. *Electrochim Acta* **2004,** *50*, 601-605.
24. Uygun, Z. O.; Uygun, H. D. E., A short footnote: Circuit design for faradaic impedimetric sensors and biosensors. *Sensors and Actuators B: Chemical* **2014,** *202*, 448-453.
25. Lee, S. J.; Mukerjee, S.; McBreen, J.; Rhob, Y. W.; Khob, Y. T.; Lee, T. H., Effects of Nafion impregnation on performances of PEMFC electrodes. *Electrochim Acta* **1998,** *43* (24), 693-701.
26. Scibioh, M. A.; Oh, I.; Lim, T.; Hong, S.; Ha, H. Y., Investigation of various ionomer-coated carbon supports for direct methanol fuel cell applications. *Applied Catalysis B: Environmental* **2008,** *77* (3-4), 373-385.
27. Ma, S.; Solterbeck, C.; Odgaard, M.; Skou, E., Microscopy studies on pronton exchange membrane fuel cell. *Appl Phys A* **2009,** *96*, 581-589.
28. Kusoglu, A.; Karlsson, A.; Santare, M.; Cleghorn, S.; Johnson, W., Mechanical response of fuel cell membranes subjected to a hygro-thermal cycle. *J Power Sources* **2007,** *161*, 987-996.
29. Norin, L.; Kostecki, R.; McLarnon, F., Study of Membrane Degradation in High Power-Lithium Ion Cells. *Electrochem Solid-State Lett* **2002,** *5* (4), A67-A69.
30. Solasi, R.; Zou, Y.; Huang, X.; Reifsnider, K.; Condit, D., On mechanical behavior and in-plane modeling of constrained PEM fuel cell membranes subjected to hydration and temperature cycles. *J Power Sources* **2007,** *167* (2), 366-377.
31. Yuan, X.; Liu, H.; Zhang, S.; Martin, J.; Wang, H., A review of polymer electrolyte membrane fuel cell durability test protocols. *J Power Sources* **2011,** *196*, 9107-9116.
32. Jourdan, M.; Mounir, H.; Marjani, R. E. In *Compilation of factors affecting durability of Proton Exchange Membrane Fuel Cell (PEMFC)*, 2014 International Renewable and Sustainable Energy Conference (IRSEC), Ouarzazate, Morocco, Ouarzazate, Morocco, 2014; pp 542-547.

33. Sethuraman, V. A.; Weidner, J. W.; Haug, A. T.; Protsailo, L. V., Durability of Perfluorosulfonic Acid and Hydrocarbon Membranes: Effect of Humidity and Temperature. *Journal of Electrochemical Society* **2008,** *155* (2), B119.
34. Dubau, L.; Castanheira, L.; Chatenet, M.; Maillard, F.; Dillet, J.; Maranzana, G.; Abbou, S.; Lottin, O.; De Moor, G.; El Kaddouri, A.; Bas, C.; Flandin, L.; Rossinot, E.; Caque, N., Carbon corrosion induced by membrane failure: The weak link of PEMFC long-term performance. *Int J Hydrogen Energy* **2014,** *39*, 21902-21914.
35. Oh, H.; Lee, J.; Kim, H., Electrochemical carbon corrosion in high temperature proton exchange membrane fuel cells. *Int J Hydrogen Energy* **2012,** *37*, 10844-10849.
36. Speder, J.; Zana, A.; Spanos, I.; Kirkensgaard, J. J. K.; Mortensen, K.; Hanzlik, M.; Arenz, M., Comparative degradation study of carbon supported proton exchange membrane fuel cell electrocatalysts – The influence of the platinum to carbon ratio on the degradation rate. *J Power Sources* **2014,** *261*, 14-22.
37. Zhang, H.; Li, J.; Tang, H.; Lin, Y., Pan, M, Hydrogen crossover through perfluorosulfonic acid membranes with variable side chains and its influence in fuel cell lifetime. *Int J Hydrogen Energy* **2014,** *39* (28), 15989-15995.
38. Spernjak, D.; Fairweather, J.; Mukundan, R.; Rockward, T.; Borup, R. L., Influence of the microporous layer on carbon corrosion in the catalyst layer. *J Power Sources* **2012,** *214*, 386-398.
39. Park, J.-H.; Yim, S.; -D; Kim, T.; Park, S.-H.; Yoon, Y.-G.; Park, G., -G; Yang, T.-H.; Park, E.-D., Understanding the mechanism of membrane electrode assembly degradation by carbon corrosion by analyzing the microstructural changes in the cathode catalyst layers and polarization losses in proton exchange membrane fuel cell. *Electrochim Acta* **2012,** *83*, 294-304.
40. Fundamentals, technology, applications. In *Handbook of fuel cells*, Wiley: Chichester, 2003; Vol. 3, p 538.
41. Dhanushkodi, S. R.; Tamb, M.; Kundu, S.; Fowler, M. W.; Pritzker, M. D., Carbon corrosion fingerprint development and de-convolution of performance loss according to degradation mechanism in PEM. *J Power Sources* **2013,** *240*, 114-121.